Polymer Chemistry

Cite this: *Polym. Chem.*, 2012, **3**, 979

www.rsc.org/polymers

PAPER

Bioactive and electroactive response of flexible polythiophene:polyester nanomembranes for tissue engineering

Maria M. Pérez-Madrigal,[ab] Elaine Armelin,*[ab] Luis J. del Valle,[a] Francesc Estrany[bc] and Carlos Alemán*[ab]

Received 9th December 2011, Accepted 10th January 2012
DOI: 10.1039/c2py00584k

Properties of free-standing nanomembranes prepared by blending poly(3-thiophene methyl acetate) and poly(tetramethylene succinate), a soluble polythiophene derivative and a biodegradable polyester, respectively, have been examined. The outstanding flexibility and robustness of the nanomembranes floating in ethanol have been demonstrated through aspiration in pipette/release/shape recovery cycles, which were repeated without cracking the film. The blend retains the electrochemical properties (*i.e.* oxidation and reduction processes) of the individual conducting polymer in both physiological and organic environments. Hydrolytic and enzymatic degradation assays show that the degradation of the polyester domains produces the detachment of the conducting polymer domains. The cellular viability, which has been studied using four different cellular lines, is significantly higher for the blend than for the polyester, indicating that the former material is a potential bioactive platform for tissue engineering. Finally, the electrobioactivity of the individual materials and the blend coated with cellular monolayers shows some dependence on the cellular line.

Introduction

Conjugated polymers (CPs) and their composites have attracted much attention because of their interesting electrical and optical properties. Indeed, these materials are currently used for a great variety of applications in different fields, like electronics, nanotechnology and biotechnology.[1–8] Among CPs, polythiophene (PTh) derivatives are particularly important since much progress has been made in the past two decades to solve their serious problems of solubility and processability.[9–11] A widely accepted strategy to overcome such problems is based on the incorporation of substituents into the 3-position of the thiophene ring. Specifically, it was found that the incorporation of long alkyl side chains increases the solubility in non-polar solvents,[12–14] whereas hydrophilic substituents produce PThs soluble in water and/or polar solvents.[15–20] For example, PThs bearing carboxylate groups, like poly(3-thiophene methyl acetate) (P3TMA), show easy solubility in different solvents and solution processability in films or fibers.[16,17,19–21]

In order to improve the mechanical integrity of CPs, in the last decade some studies have been focused on blends of PTh derivatives with conventional polymers. Hsieh *et al.* studied the miscibility of poly(3-thiophene acetic acid) with poly(ethylene oxide), films being obtained by solvent casting polymer solutions onto a glass plate.[22] Nicho *et al.* studied the morphological and physicochemical properties of thin film composites made of poly(3-octylthiophene) and polystyrene, which were spin-coated onto corning glass substrates from toluene.[23] Özgün *et al.* characterized blends and composites with different molar ratios of PTh and polyoxymethylene.[24] More recently, Manna *et al.* fabricated new nanostructures of poly(3-thiophene methyl acetate) within a poly(vinylidene fluoride) matrix using a reactive blending technique under melt-cooled conditions.[25] Finally, Mawad *et al.* prepared a multilayered system based on water soluble polymers with charges of opposite sign, poly[(3-thienyl) ethoxypropanesulfonate] and poly(ethyleneimine), electrostatically assembled by the layer-by-layer technique.[26]

Among CP applications, those related with both biotechnology and biomedicine have a very relevant impact. More specifically, CPs are biocompatible materials able to stimulate cell attachment, proliferation, regeneration and differentiation through electrical signals and/or simple ion-exchange in which the dopant agents embedded in the material play a crucial role.[27–33] Although these properties favor the use of CPs as scaffolds for tissue engineering, the biomedical use of these materials is still limited because of their lack of biodegradability. Combination of thiophene and pyrrole units with an aliphatic moiety, which acts as a linker, allowed Rivers *et al.* to obtain a biodegradable CP.[34]

Motivated by both the mechanical integrity provided by the mixture of CPs with conventional insulating polymers and the

[a]*Departament d'Enginyeria Química, E.T.S d'Enginyers Industrials de Barcelona, Universitat Politècnica de Catalunya, Av. Diagonal 647, Barcelona E-08028, Spain. E-mail: elaine.armelin@upc.edu; carlos.aleman@upc.edu*
[b]*Center for Research in Nano-Engineering, Universitat Politècnica de Catalunya, Campus Sud, Edifici C', C/Pasqual i Vila s/n, Barcelona E-08028, Spain*
[c]*Departament d'Enginyeria Química, Escola Universitària d'Enginyeria Tècnica Industrial de Barcelona, Universitat Politècnica de Catalunya, Comte d'Urgell 187, 08036 Barcelona, Spain*

necessity of biodegradable CPs, we recently reported the fabrication of free-standing nanomembranes made of a PTh derivative and a polyester.[35] Specifically, nanomembranes were prepared by spin-coating blended solutions of P3TMA, a soluble PTh derivative, and poly(tetramethylene succinate) (PE44), a biodegradable polyester. The thickness of these ultra-thin films, which were stable in both air and ethanol solution for more than a year, ranged from 20 to 80 nm while the area varied between 4 and 50 cm^2 depending on the dimensions of the substrate used in the spin-coating process. Thermal, morphological and electrical properties of the P3TMA:PE44 nanomembranes were described in our previous study.[35] Furthermore, we also reported preliminary qualitative studies about both the enzymatic degradation with Lipase F-AP 15 from *Rhizopus oryzae* and the bioactive behavior against human laryngeal epidermoid carcinoma (HEp-2) cells of such nanomembranes. The promising results derived from such studies have motivated the present work, in which we examine the following items related with the P3TMA:PE44 nanomembranes: (i) the intrinsic electrochemical properties, which have remained completely unknown; (ii) the hydrolytic and enzymatic degradability, both from a quantitative point of view; (iii) the response towards different fibroblast and epithelial cellular lines using both adhesion and proliferation studies; and (iv) the electrobioactivity, which has allowed us to determine the influence of cell monolayers in the electrochemical characteristics. It should be noted that this work has been mainly focused in nanomembranes obtained using a 50 : 50 P3TMA:PE44 molar ratio, which was found to present better performance than the 20 : 80 and 80 : 20 ones.[35]

Methods

Materials

3-Thiophene acetic acid (3TAA) (98.0%) and poly(4-hydroxysytrene) (PHS) (M_w *ca.* 11 000) were purchased from Fluka (Poland) and Sigma-Aldrich (USA), respectively. Iron chloride anhydrous (97.0%), dry methanol (99.5%), ethanol (99.5%), chloroform (99.9%) and acetonitrile (analytical reagent grade) were all purchased from Panreac Quimica S.A.U. (Spain) and used as received without further purification.

For cell culture experiments, Madin Darby canine kidney (MDCK), human prostate cancer (Du-145), human laryngeal epidermoid carcinoma (HEp-2) and monkey kidney fibroblast (Cos-7) cells were purchased from ATCC (USA). Dulbecco's phosphate buffered saline solution (PBS) without calcium chloride and magnesium chloride, Dulbecco's modified Eagle's medium (DMEM, with 4500 mg of glucose L^{-1}, 110 mg of sodium pyruvate L^{-1} and (2 mM) L-glutamine), penicillin–streptomycin, 3-(4,5-dimethylthiazol-2-yl)-2,5-diphenyltetrazolium bromide (MTT, 97.5%) and trypsin–EDTA solution (0.05% trypsin, 0.02% EDTA) were all purchased from Sigma-Aldrich (USA). Fetal bovine serum (FBS) and trypan blue stain (0.4%) were purchased from Gibco, UK. Dimethyl sulfoxide (99.0%) was purchased from Panreac Quimica S.A.U. (Spain) and sodium azide (NaN_3, ≥99.5%) from Sigma-Aldrich (USA). Finally, Lipase F-AP 15 (from *Rhizopus oryzae*) was purchased from Sigma (USA) and used in the enzymatic degradation experiments.

Synthesis of poly(3-thiophene methyl acetate) and poly(tetramethylene succinate)

Soluble P3TMA was prepared by oxidative coupling polymerization of 3-thiophene methyl acetate (3TMA),[16] the latter being obtained using 3TAA as a starting monomer. On the other hand, biodegradable PE44 was prepared by bulk thermal polycondensation of 1,4-butanediol and succinic acid (diol/diacid molar ratio of 2.2/1).[36] The synthetic routes of the two polymers are summarized in Scheme 1. Chemical characterization, viscosities and molecular weights were reported in our previous study.[35]

Fabrication of P3TMA:PE44 50 : 50 nanomembranes

The procedure for the fabrication of P3TMA:PE44 nanomembranes, which was based on that described by Kunitake and co-workers[37–39] for the preparation of ultrathin films of epoxy resins, was optimized in our previous work.[35] Nanomembranes for quantitative degradation assays were prepared using a sacrificial layer, which facilitated the detachment from the substrate, as follows. An ethanol solution of PHS (50 mg mL^{-1}) was firstly spin-coated on an indium-tin oxide (ITO) glass slide (dimensions ranged from 2.5 × 2.5 cm^2 to 3.0 × 5.0 cm^2) at 3000 rpm for 60 s to give a 0.1 mm thick sacrificial layer. After this, chloroform solutions of P3TMA and PE44 (50 mg mL^{-1}) were prepared and subsequently mixed in a 50 : 50 molar ratio. The mixture was stirred with a magnetic stirrer at room temperature for 4 h, diluted five times with chloroform and filtered prior to spin-coating. Next, the mixture solution was spin coated at 3000 rpm for 60 s. Later, the spin coated substrates were dried under vacuum at room temperature for 24 h to remove completely the solvent. Detachment of the nanomembranes from the ITO substrate was achieved by immersion into ethanol, the edges of the specimen being finely cut in order to facilitate the penetration of the solvent into the sacrificial layer for its dissolution. Nanomembranes were also fabricated using steel AISI 316 sheets (dimensions 1.0 × 1.0 cm^2) as substrate using the same procedure. Detachment of the nanomembranes from the substrate was not required for some assays (*i.e.* cellular adhesion and proliferation), no sacrificial layer being necessary in such cases. Accordingly, film deposition on the substrate was directly carried out by spin-coating the P3TMA:PE44 mixture solution at 3000 rpm for 60 s. The average thickness measured by AFM and SEM of the ultrathin films fabricated using this procedure was 15 nm and 19 nm, respectively.

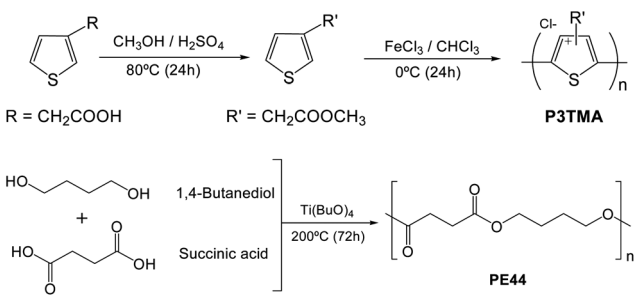

Scheme 1 Synthesis of P3TMA and PE44.

Spin-coating was performed using a Spin Coater (WS-400BZ-6NPP/A1/AR1, Laurell Technologies Corporation).

FTIR spectroscopy

IR absorption spectra were recorded on a FTIR Jasco 4100 spectrometer. Samples were placed in an attenuated total reflection accessory (top-plate) with a diamond crystal (Specac model MKII Golden Gate Heated Single Reflection Diamond ATR). PE44 and P3TMA:PE44 films were prepared by solvent casting from the corresponding chloroform solutions while P3TMA was analyzed as a powder. For each sample 32 scans were performed between 4000 and 600 cm^{-1} with a resolution of 4 cm^{-1}.

Electrochemical assays

The electrochemical behavior of the nanomembranes was investigated by cyclic voltammetry (CV) using both acetonitrile and PBS (pH = 7.4) solutions. Measurements were performed on ultra-thin films, which were deposited on steel sheets by spin-coating, before and after covering them with cells.

All electrochemical assays were performed with a VersaStat II potentiostat–galvanostat (Princeton Applied Research) using a three-electrode compartment cell under nitrogen atmosphere (99.995% pure) at room temperature. The working compartment was filled with 50 mL of electrolyte solution (acetonitrile or PBS) with 0.1 M $LiClO_4$ as supporting electrolyte, while the cathodic compartment was filled with 10 mL of the same electrolyte solution. Steel AISI 316 sheets of 1.0 × 1.0 cm^2 in area were used as working and counter electrodes. The reference electrode was an Ag|AgCl electrode containing a KCl saturated aqueous solution (offset potential *versus* the standard hydrogen electrode, E^0 = 0.222 V at 25 °C), which was connected to the working compartment through a salt bridge containing the electrolyte solution.

The initial and final potentials were −0.40 V, whereas a reversal potential of 1.20 and 1.10 V was considered for PBS and acetonitrile, respectively. Scan rates of 10, 25 and 50 mV s^{-1} were used in this work. The electroactivity (*i.e.* ability to store charge) increases with the similarity between the anodic and cathodic areas of the first control voltammogram, whereas the electrostability (*i.e.* electrochemical stability) decreases with the oxidation and reduction areas of consecutive control voltammograms.

Contact angle measurements

Contact angles were obtained using the water drop method. Images of water drops (3 μL) in the surface of the films were recorded with a contact angle meter (Dataphysics, Contact Angle System OCA15+) after stabilization (30 s). The images of the drop shapes were analysed, and the contact angle measures were carried out with the SCA20 software. Measurements were performed four times for each material.

Hydrolytic degradation studies

Degradation studies were carried out on both films prepared by solvent casting and cut to approximately 1 cm × 1 cm and nanomembranes deposited on steel substrates, the former and the latter being used for quantitative (weight loss) and qualitative (SEM studies) analyses. Both films and nanomembranes were placed in vials containing 10 mL of PBS solution supplemented with 0.1 mg mL^{-1} of sodium azide, and incubated at 37 °C in a shaking incubator set at 100 rpm for a total of eight weeks. Vials were closed and sealed with parafilm to avoid loss of solution by evaporation, even though the PBS solution was replaced every 48 h. Samples were analyzed after 4 days, 7 days, 2 weeks, 4 weeks and 8 weeks.

After each immersion time, samples were removed from the solution and gently washed with distillated water. After drying under vacuum for several days at room temperature (24 h), films were weighed. Degradation was quantitatively monitored as weight loss (WL, in %) of the films by applying the following formula:

$$\mathrm{WL} = \frac{m_0 - m_t}{m_0} \times 100$$

where m_0 is the weight of the film before the degradation assay and m_t is the weight of the film after exposure to the degradation medium. The influence of the hydrolytic degradation on the morphology was evaluated by SEM. For SEM studies, nanomembranes were sputter-coated with carbon before observation.

Enzymatic degradation studies

The procedure was identical to that mentioned above for hydrolytic degradation studies with exception of the solution contained in the vials, which was formed by 4 mg mL^{-1} of Lipase F-AP 15 in a 10 mL of PBS solution supplemented with 0.1 mg mL^{-1} of sodium azide to prevent contamination. The variation of the weight loss against the exposure time was used to evaluate the enzymatic degradability from a quantitative point of view.

Cell adhesion and proliferation tests

MDCK, Du-145, HEp-2 and Cos-7 cells were cultured in DMEM high glucose supplemented with 10% FBS, penicillin (100 units per mL), and streptomycin (100 μg mL^{-1}). The cultures were maintained in a humidified incubator with an atmosphere of 5% CO_2 and 95% O_2 at 37 °C. Culture media were changed every two days. When the cells reached 80–90% confluence, they were detached using 1–2 mL of trypsin (0.25% trypsin/EDTA) for 5 min at 37 °C. Finally, cells were resuspended in 5 mL of fresh medium, their concentration being determined by counting in a Neubauer camera using 0.4% trypan blue as a dye vital.

Nanomembranes of PE44, P3TMA and 50 : 50 P3TMA:PE44 were prepared and deposited onto steel AISI 316 sheets of 1 cm^2. These samples were placed in plates of 24 wells and sterilized using UV-light for 15 min in a laminar flux cabinet. Controls were simultaneously performed by culturing cells on the surface of the tissue culture polystyrene (TCPS) plates and steel plates. For adhesion assays, an aliquot of 50 μL containing 5 × 10^4 cells was deposited on the nanomembrane of each well. Then, cell attachment to the nanomembrane surface was promoted by incubating under culture conditions for 30 min. Finally, 500 mL of the culture medium were added to each well. After 24 h, non-attached cells were washed out while attached cells were

quantified. For proliferation assays, the 50 μL aliquots deposited on each well contained 2×10^4 cells, quantification of proliferated cells being performed after 7 days of culture.

Cell adhesion and proliferation were evaluated by the colorimetric MTT assay.[40] This assay measures the ability of the mitochondrial dehydrogenase enzyme of viable cells to cleave the tetrazolium rings of the MTT and form formazan crystals, which are impermeable to cell membranes and, therefore, are accumulated in healthy cells. This process is detected by a color change: the characteristic pale yellow of MTT transforms into the dark blue of formazan crystals. Specifically, 50 mL of MTT solution (5 mg mL^{-1} in PBS) were added to each well. After 3 h of incubation, samples were washed twice with PBS and stored in clean wells. In order to dissolve formazan crystals, 1 mL of DMSO/methanol/water (70/20/10% v/v) was added. Finally, the absorbance at 540 mm was measured after using an UV-vis spectrophotometer (UV-3600, Shimadzu). The resulting viability results were normalized to TCPS control as relative percentages.

Results were derived from the average of four replicates ($n = 4$) for each independent experiment. ANOVA and Tukey tests were performed to determine the statistical significance, which was considered at a confidence level of 95% ($p < 0.05$).

Microscopy

Micrographs were taken with a Canon IXUS 40 digital camera. SEM observations were carried out using a Focused Ion Beam Zeiss Neon40 scanning electron microscope equipped with an energy dispersive X-ray (EDX) spectroscopy system and operating at 5 kV. All samples were coated with a carbon layer of 6 nm thickness using a K950X Turbo Evaporator to prevent sample charging problems. Before the carbon coating for examination by SEM, samples covered with cells were fixed in a 2.5% glutaraldehyde PBS solution (pH = 7.2) overnight at 4 °C. Then, they were dehydrated by washing in an alcohol battery (30°, 50°, 70°, 90°, 95° and 100°) at 4 °C for 30 min per wash. Finally, samples were air-dried, and sputter-coated with carbon before SEM observation.

Results and discussion

Nanomembranes

Fig. 1a shows a digital camera image of a nanomembrane immersed in ethanol, which was fabricated and detached using the procedure previously described. The average thickness of the 50 : 50 nanomembranes was measured to be $\ell = 15$ and 19 nm by AFM scratch and SEM, respectively.[35] These self-standing PT3MA:PE44 nanomembranes are very flexible and robust, their folding into small shapes being an easy process. This is evidenced in Fig. 1b–i, which show optical images of the aspiration process of a nanofilm, with an area of 5 cm^2 floating in ethanol, into a pipette with a tip diameter of 1 mm. As can be seen, the nanomembrane is completely introduced into the pipette (Fig. 1f) due to its outstanding flexibility. After releasing it into the solvent, the nanofilm adopts a folded appearance (Fig. 1g)

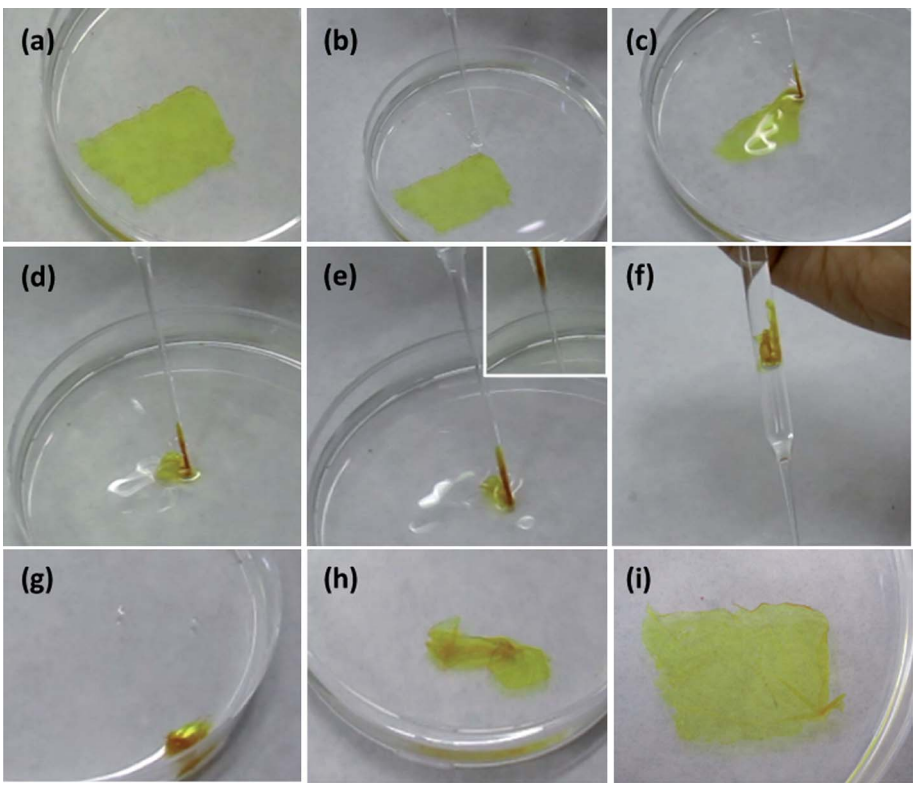

Fig. 1 (a) Digital camera image of a P3TMA:PE44 free-standing nanomembrane immersed in ethanol; (b–f) aspiration of the nanomembrane floating in ethanol into a pipette; (g–h) release of the folded nanomembrane into the ethanol solution; and (i) aspect of the nanomembrane after recovering the shape.

recovering rapidly its original shape when manipulated with a spatula (Fig. 1i). This aspiration/release/shape recovery process can be repeated more than five times without producing any damage in the nanomembrane. A similar behaviour was reported for hybrid inorganic/organic hybrid nanomembranes made of zirconia and a crosslinked polymer,[37] their robustness and flexibility being essentially attributed to the combination of hard and soft networks in a single material. Thus, in that case two-dimensionally extended double interpenetrated networks were used to reinforce the mechanical properties of the hybrid nanomembrane. However, it should be emphasized that the 50 : 50 P3TMA:PE44 is a pure organic blend without crosslinkings. Accordingly, the robustness and flexibility of the nanomembranes studied in this work are due to the excellent dispersion achieved between the two organic materials.

Fig. 2 compares SEM images of P3TMA, PE44 and P3TMA:PE44 50 : 50. A detailed description of the morphologies of such three materials was provided in our previous work[35] and, therefore, discussion has been restricted here to a brief summary necessary for understanding degradation effects. The micrograph of the individual CP (Fig. 2a) shows spherical cavities of nanometric dimensions, which have been attributed to the detachment of nanoparticles formed by molecular aggregations. The morphology of the polyester (Fig. 2b), which in opposition to P3TMA presents excellent film forming properties, corresponds to superficial packing of lamellar aggregates. P3TMA:PE44 nanomembranes (Fig. 2c) show a homogeneous distribution of spherical phases, which correspond to nanoaggregates of the CP, embedded in the polyester matrix.

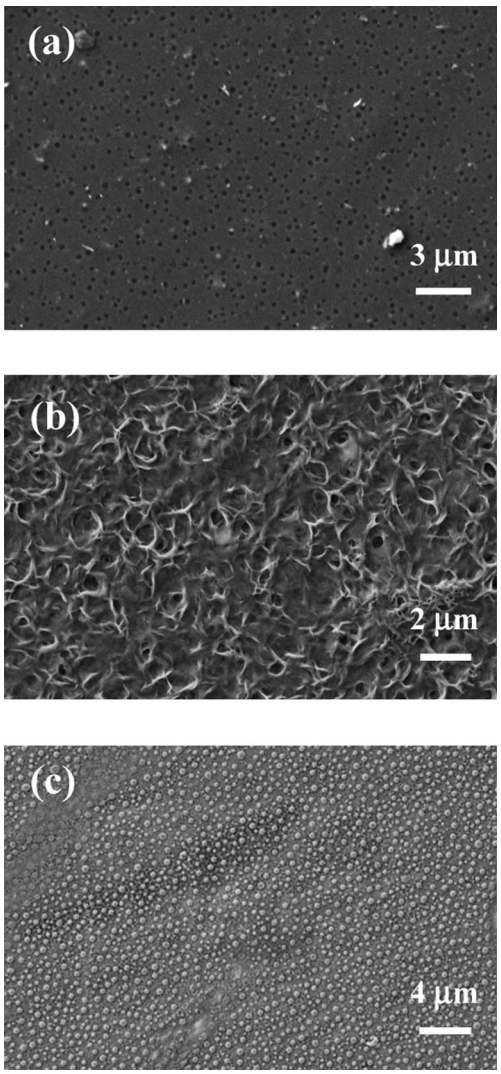

Fig. 2 SEM micrographs of nanomembranes made of: (a) P3TMA, (b) PE44 and (c) P3TMA:PE44 mixture with 50 : 50 molar ratio.

Fig. 3 shows the FTIR spectrum of P3TMA, PE44 and 50 : 50 P3TMA:PE44 in the range 1800–550 cm^{-1}. Changes and shifts occurring at higher wavenumbers are not displayed but discussed for comparison. Absorption bands of the two individual polymers and the three blends (20 : 80, 50 : 50 and 80 : 20 P3TMA:PE44 compositions) are displayed in Table 1. Although CPs are difficult to identify by infrared spectroscopy, some assessments can be pointed out. The band for C–H aromatic stretching vibration is only observed in the P3TMA spectrum (3005 cm^{-1}), and it is associated with the benzonoid or quinonoid form. Other C–H stretching vibrations are identified for the aliphatic segment (2998, 2948, and 2843 cm^{-1}). The weak absorption intensity at 1522 cm^{-1} has been attributed to C=C stretching vibration of the thiophene ring, indicating the conjugation behaviour of P3TMA chains. Another C=C aromatic ring stretching (medium intensity) is observed at 1322 cm^{-1}. Asymmetric and symmetric stretching of ester groups in P3TMA are identified at 1146 cm^{-1} (C=O, broad and high intensity), 1196 cm^{-1} (R–CO–O–CH_3, weak intensity) and 1013 cm^{-1} (C–O–C, broad and medium intensity). Finally, the peak at 615 cm^{-1} has been attributed to the C–S bonds of the thiophene rings.

On the other hand, the main absorption bands corresponding to C–H aliphatic stretching of PE44 are observed at 2964, 2946 and 2857 cm^{-1}. Absorption bands characteristic of $-(CH_2)_n-$ hydrocarbon chains are detected at 804 cm^{-1} (sharp) and 748 cm^{-1} (broad, CH_2 rock vibrations). Relevant bands related to the CH_2 asymmetric and symmetric bending are shown

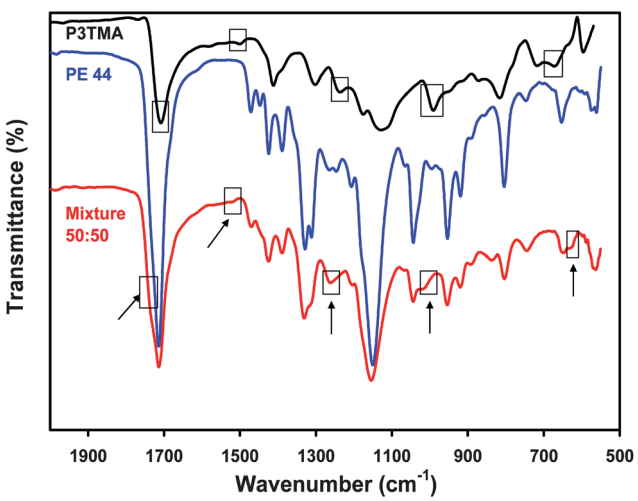

Fig. 3 FTIR spectrum of P3TMA, PE 44 and 50 : 50 P3TMA:PE44 in the range 1800–550 cm^{-1}. Absorption bands marked with boxes and arrows have been used to identify the conducting polymer in the mixture (see text).

Table 1 Main infrared absorption bands (cm^{-1}) of P3TMA, PE44 and P3TMA:PE44 (50 : 50) blend studied in this work

Compound	Aromatic C–H in plane deform.	Aliphatic C–H stretch	C=O ester	C=C conjugated diene	CH_3 asymmetric symmetric bending	CH_2 asymmetric symmetric bending	C–O–C stretches	Aliphatic C–H out of plane bending	Aromatic C–H out of plane deform.	
	β								α	β
P3TMA	3005	2998, 2948, 2843	1726	1690[a], 1522, 1322	1431	1402	1196, 1148 (broad and strong), 1016	689	737	835
P3TMA:PE44 (80 : 20)	~3000	2937, 2836	1713	1510	1421	1422, 1381, 1312	1190, 1141, 1109	681	726	830
P3TMA:PE44 (50 : 50)	—	2948, 2919, 2858	1732, 1713	1675[a]	1444	1470, 1424, 1389, 1331, 1314	1043, 1018, 1016		743	836
P3TMA:PE44 (20 : 80)	—	2934, 2904, 2896	1708	—	—	1460, 1418 1383, 1322, 1251	1147, 1036, 948	800, 642	738	837
PE44	—	2964, 2946, 2923, 2857	1714	—	—	1472, 1448, 1424, 1389	1329, 1311 (doublet) 1207,1150 (strong), 1044, 954	804, 748, 653	—	—

[a] Band overlapped with C=O ester.

between 1470 and 1390 cm^{-1}. Three significant peaks are detected in the PE44 spectrum at 1150 cm^{-1} (sharp and strong absorption band), 1044 and 954 cm^{-1} (sharp and medium absorption bands), which have been assigned to the C=O and C–O–C vibrations. Other bands typically associated with the C–O component tend to be less pronounced, sometimes being overlapped with other fingerprint absorptions of the molecule. These bands are usually located in the 1320–1200 cm^{-1} (C–O stretch) interval. In the current case, they appear as sharp and strong doublet bands at 1329 and 1311 cm^{-1}; and also at 954 cm^{-1}, as discussed above.

Formation of 50 : 50 P3TMA:PE44 nanomembranes is evidenced by some overlapped bands, which are marked in Fig. 3, arising from the two individual polymers. The strong absorption at 1716 cm^{-1} and the broad shoulder at 1734 cm^{-1} have been attributed to the C=O stretching of ester units from PE44 and P3TMA, respectively. Furthermore, a very weak shoulder at 1508 cm^{-1} was also observed for the mixture, corresponding to the C=C stretching of thiophene ring. Other overlapped bands arising from the P3TMA contribution can be seen at: 1262, 1018, 837 and 620 cm^{-1}. Similar features are displayed in Table 1 for the 20 : 80 and 80 : 20 nanomembranes.

The contact angles of steel, P3TMA, PE44 and 50 : 50 P3TMA:PE44 have been determined to illustrate the morphological changes induced by the blending on the wettability of the films. The contact angle of P3TMA at room temperature is $\theta = 93.8 \pm 3.46°$. This value indicates that the hydrophobicity at the surface of P3TMA is significantly higher than that observed for other polythiophene derivatives (*e.g.* $\theta = 54.0 \pm 0.6°$ for poly(3,4-ethylenedioxythiophene)[41]). On the other hand, the contact angles of PE44 and steel are $\theta = 76.1 \pm 2.5°$ and $31.2 \pm 0.0°$, indicating that the two materials, especially the latter, are considerably more hydrophilic than the CP. Finally, the contact angle of the 50 : 50 PT3MA:PE44, $\theta = 91.9 \pm 1.8°$, is very close to that of the individual CP. This result is fully consistent with the SEM image of the blend displayed in Fig. 2c, which allows identification of spherical P3TMA nanoparticles trapped in the polyester matrix. Thus, the phase separation between the two components of the blend is the cause of the fundamental role played by the CP in the wettability of the film surface.

Electrochemical behavior of the nanomembranes

The intrinsic electrochemical properties of the blend and the individual polymers were investigated in both PBS and acetonitrile solutions, 0.1 M $LiClO_4$ being added in both cases as supporting electrolyte. Control voltammograms recorded for P3TMA, PE44 and 50 : 50 P3TMA:PE44 in PBS and acetonitrile are compared in Fig. 4a and b, respectively. Voltammograms collected using scan rates of 10 and 50 mV s^{-1} are displayed to provide information about the definition of the peaks. In general, the oxidation and reduction peaks are more clear and intense in acetonitrile than in PBS indicating that polarons are formed at more specific positions of the polymer chains in the former environment than in the latter one.

The electroactivity of chemically produced P3TMA is significantly higher in the organic solvent than in PBS, which is consistent with preliminary investigations reported for the electrochemically polymerized material 3TMA.[42] In PBS the CP shows an oxidation shoulder O_1 with anodic peak potential

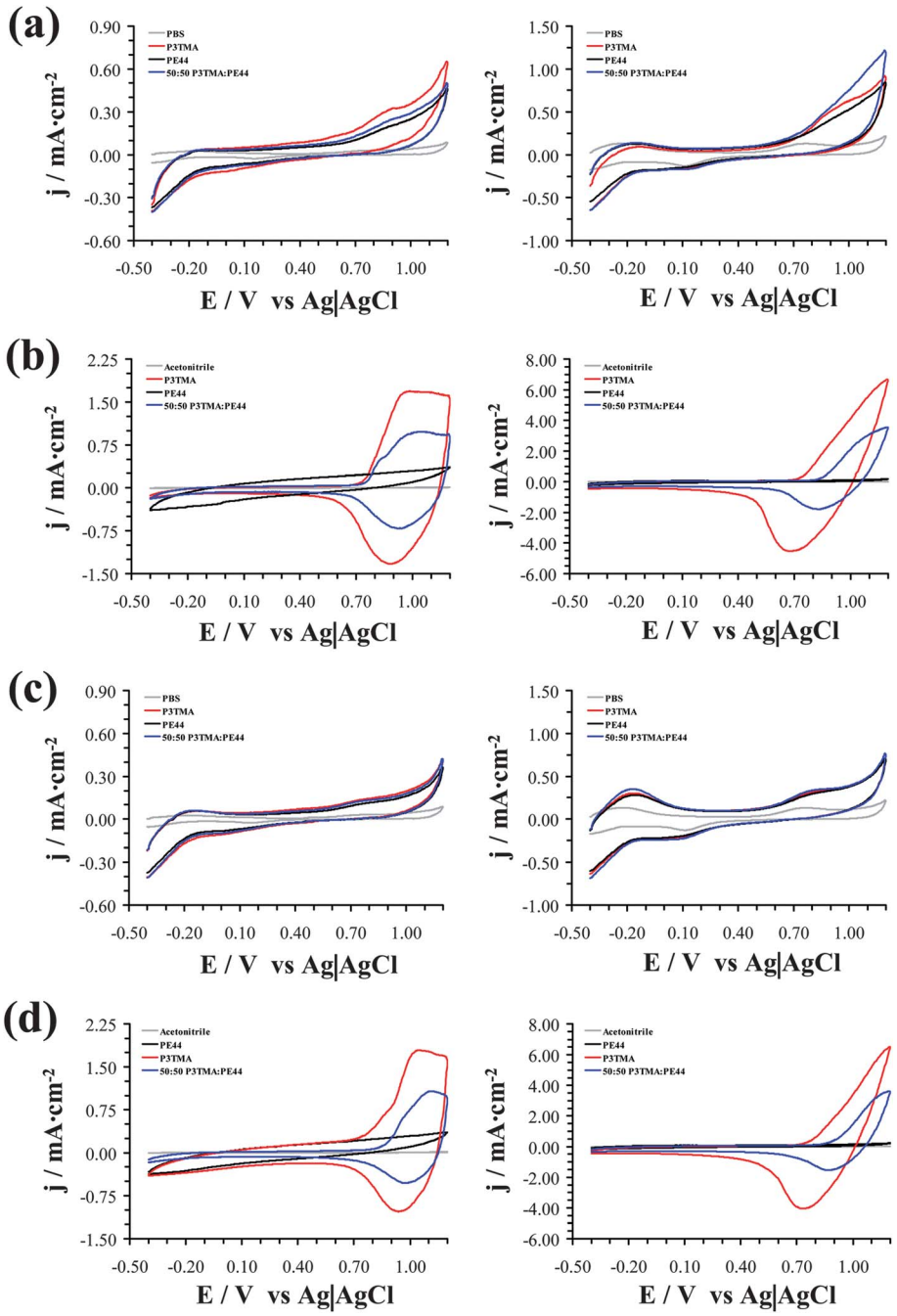

Fig. 4 Control voltammograms collected using scan rates of 10 and 50 mV s^{-1} (left and right, respectively) of P3TMA, PE44 and 50 : 50 P3TMA:PE44 in (a) PBS and (b) acetonitrile solutions with 0.1 M $LiClO_4$. Control voltammograms of the same species after 10 consecutive oxidation–reduction cycles in (c) PBS and (d) acetonitrile solutions with 0.1 M $LiClO_4$.

$E_p^a(O_1) = 0.84$ V, and an oxidation peak O_2 that is expected to reach an anodic peak potential $E_p^a(O_2) \approx 1.4$ V (*i.e.* 0.20–0.25 V above the reversal potential). These two processes, which have been attributed to the formation of polarons and bipolarons in polymer chains, are highly irreversible. Thus, the cathodic scan shows a weak reduction shoulder R_1 with a cathodic peak potential of −0.14 V.

The anodic scan recorded for P3TMA in acetonitrile indicates that at potentials around 0.7 V begins a very clear oxidation peak, O_2, which is expected to show an anodic peak potential $E_p^a(O_2) \approx 1.5$ V (*i.e.* ~0.3 V above the reversal potential). An oxidation shoulder, O_1, partially overlapped with O_2 is detected at potentials close to 1.0 V. These results indicate the formation of polarons and bipolarons in the polymeric chains at ~1.0 and ~1.5 V, respectively. Moreover, comparison of the current densities indicates that the amount of oxidized molecules is significantly larger in acetonitrile than in PBS. Thus, in acetonitrile the current density for O_3 at 1.20 V is 6.61 mA cm^{-2}, whereas in PBS the current density at 1.20 V is 0.91 mA cm^{-2}. The cathodic scan in acetonitrile reflects a reduction peak R_1

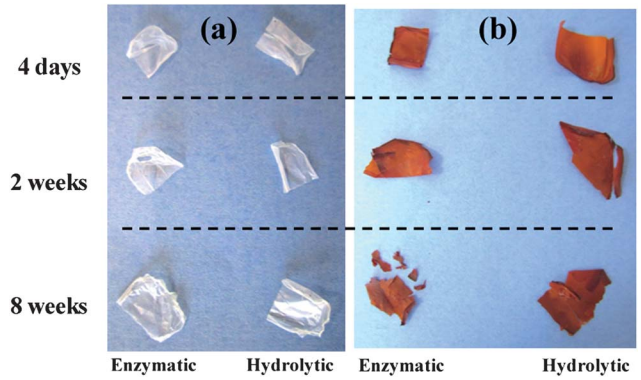

Fig. 5 Optical photographs showing the (a) PE44 and (b) 50 : 50 P3TMA:PE44 samples after 4 days, 4 weeks and 8 weeks of hydrolytic and enzymatic degradation.

with $E_p^c(R_1) = 0.88$ V (*i.e.* polarons and bipolarons reduce at the same potential). These features suggest the formation of a quasi-reversible redox pair in acetonitrile. Moreover, the voltammogram of the blank demonstrates that the identified shoulders and peaks are not perturbed by the organic solvent.

The voltammogram recorded for PE44 in PBS is similar to that recorded for P3TMA in the same medium. Thus, the oxidation shoulder O_1 with $E_p^a(O_1) = 0.90$ V and the oxidation peak O_2 with an anodic peak potential higher than 1.20 V have been attributed to the formation of irreversible polarons and bipolarons, respectively. The cathodic scan shows a small reduction shoulder R_1 with cathodic peak potential $E_p^c(R_1) = 0.10$ V, which corresponds to the reduction of PBS. The voltammogram recorded for PE44 in acetonitrile does not show oxidation or reduction processes, indicating that no oxidized specie is formed in the potential range from −0.50 to 1.20 V.

The behavior of the 50 : 50 P3TMA:PE44 mixture in both PBS and acetonitrile shares some of the characteristics discussed for the two individual components, even though some distinctive features are also reflected. In PBS the oxidation peak O_1 shows an anodic peak potential, $E_p^a(O_1) = 0.75$ V, lower than those of the two individual polymers. However, the characteristics of O_2 and R_1 are similar to those described for P3TMA and PE44 in this medium, confirming that the irreversibility of the oxidation processes is maintained in the blend. The voltammogram recorded for the blend in acetonitrile presents an oxidation peak that begins at 0.80 V and is expected to present an anodic peak potential ~0.3 V higher than the reversal potential. This peak has been associated with the oxidation peak O_2 of P3TMA, even though the current density at 1.20 V is lower for the blend than for the individual CP (1.35 and 2.60 mA cm^{-2}, respectively). The cathodic scan of the blend presents a reduction peak with a cathodic peak potential of 0.90 V, which corresponds to the peak R_1 identified for the pure CP, indicating the formation of polarons in P3TMA molecules.

Fig. 4c and d show the voltammograms recorded for P3TMA, PE44 and 50 : 50 P3TMA:PE44 in PBS and acetonitrile, respectively, with 0.1 M $LiClO_4$ after ten consecutive oxidation–reduction cycles. As can be seen, the integrated cathodic and anodic areas decrease, independently of the environment, after such amount of cycles indicating a reduction of the electroactivity. However, the electrochemical stability of the blend has been found to be similar in PBS and acetonitrile. The quantitative determination of the loss of electroactivity for the two electroactive species (*i.e.* P3TMA and 50 : 50 P3TMA:PE44) is around 40% and 30% in PBS and acetonitrile, respectively.

Hydrolytic degradation

Fig. 5 compares the PE44 and 50 : 50 P3TMA:PE44 films after 4 days, 2 weeks and 8 weeks of immersion in PBS solution. As can be seen, the mechanical integrity of the PE44 films was retained in all cases. However, the SEM micrographs of PE44 nanomembranes (Fig. 6a and b) suggest that the influence of the PBS solution on the surface morphology is non-negligible after 4 and 8 weeks of exposure. Thus, degradation produces changes in the superficial texture of the polyester and numerous crevasses and thin grooves appear, their extension and proportion being more noticeable as the immersion time increases. When an aliphatic polyester is submerged in an aqueous environment, the water only penetrates into the amorphous domains of the polymer chains; it cannot enter the crystalline regions, as reported elsewhere.[43] Amorphous domains can undergo surface erosion or bulk degradation. A theoretical model supported experimentally was developed to predict the erosion mechanism of water

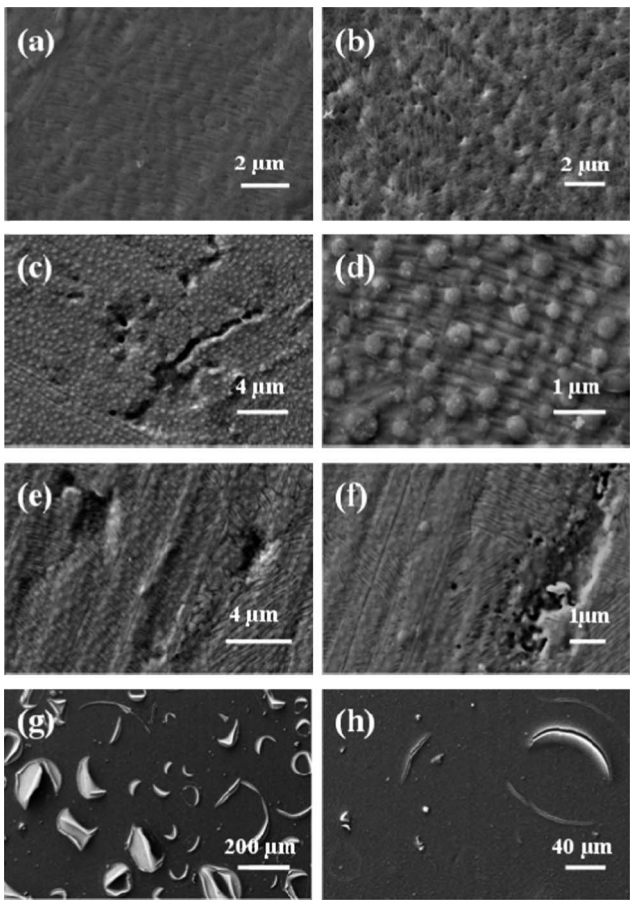

Fig. 6 SEM micrographs of hydrolytically degraded nanomembranes: PE44 after 4 weeks (a) and (b) 8 weeks of immersion; 50 : 50 P3TMA:PE44 after 4 weeks (c and d) and 8 weeks (e and f) of immersion; low (g) and high (h) resolution micrographs of P3TMA after 8 weeks of immersion.

insoluble biodegradable polymer matrices.[44] The model showed that the type of degradation depends on the diffusivity of water inside the matrix, the degradation rate of the polymer's functional groups and the matrix dimensions, these parameters allowing a critical device dimension L_c to be calculated. If the matrix dimensions are larger than L_c it will be subjected to surface erosion, otherwise it will undergo bulk erosion. The influence of L_c on the degradation was experimentally confirmed using poly(α-hydroxy ester) matrices.[44] Experiments on other aliphatic polyesters also showed bulk erosion processes.[45–47] Koning and co-workers demonstrated that the main reaction in the degradation of aliphatic polyesters is the autocatalytic hydrolysis of ester bonds, which causes the molecular weight to decrease.[48,49] The reduction of the molecular weight has been measured using films prepared by solvent casting (see the Methods section) and determining the temporal evolution of the weight loss (WL). As can be seen in Fig. 7, the weight remains practically unaltered after 8 weeks of immersion in PBS (*i.e.* WL = 1.4%) indicating that the changes in superficial texture only correspond to the first stages of the degradation process.

Hydrolytic degradation underwent by 50 : 50 P3TMA:PE44 nanomembranes resembles that observed for the polyester. Thus, the appearance of abundant crevasses and thin grooves was detected after 4 weeks of immersion in PBS (Fig. 6c and d), these effects becoming more pronounced after 8 weeks (Fig. 6e and f). However, Fig. 7 indicates that changes in the superficial texture are accompanied by a significant increase of the weight loss (WL = 17.2%). Thus, we found that the degradation of the polyester in the blend produced the detachment of the P3TMA domains, the thin grooves observed after 4 weeks of degradation transform into large and deep cracks after 8 weeks. Moreover, the mechanical integrity of P3TMA:PE44 disappears after two weeks, hydrolytic degradation inducing the fragmentation of the films (Fig. 5). These results indicate that the contribution of the polyester is essential not only to provide mechanical integrity but also to facilitate the hydrolytic degradation of the P3TMA:PE44 nanomembranes.

Immersion of P3TMA in PBS produced a delamination process, which is evidenced in the SEM micrographs displayed in Fig. 6g and h. This particular degradation process, which started after 2 weeks, was initially observed through the appearance of blisters and small cracks around them. However, inspection of the samples submerged during 8 weeks reflected significant growth of such cracks, which induced the above-mentioned delamination process. Thus, fragments of relatively large dimensions were released to the medium, leaving holes that are detectable at first glance (*i.e.* visible to the naked eye). The delamination process, which is not properly a degradation process, of P3TMA may be attributed to a corrosion process at the steel substrate, which was used to deposit the material. More specifically, molecules of water, which were absorbed by the nanofilm due to the hydrophilic carboxylate side groups, reached the steel/P3TMA interface. This absorption produced not only a swelling effect but also the corrosion of the anodic region (*i.e.* in the metal surface, under the P3TMA coating), which was activated by the dissolved salts. These features enabled the development of blisters and tensions on the surface, inducing the formation of crevasses in the nanomembrane. Interestingly, the delamination process described for P3TMA was not observed in P3TMA:PE44 nanomembranes. Due to the apparition of this phenomenon, no quantitative analysis of the degradation was carried out for P3TMA.

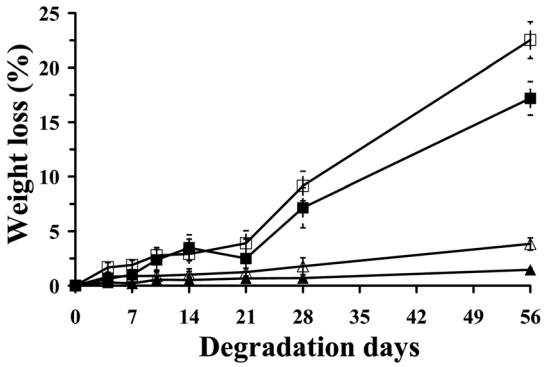

Fig. 7 Plot of the weight loss (%) *versus* the degradation time (days) in hydrolytic (filled symbols) and enzymatic media (empty symbols) for PE44 (triangles) and 50 : 50 P3TMA:PE44 (squares) films.

Enzymatic degradation

Results derived from enzymatic degradation assays are qualitatively similar to those described above for hydrolytic degradation but quantitatively enhanced due to the action of the enzyme. This qualitative similarity is reflected in both the digital camera images displayed in Fig. 5, which compares the effects of the two different degradation media in the PE44 and 50 : 50 P3TMA:PE44 films, and the SEM micrographs (not shown). Thus, although PE44 films retain the mechanical integrity after 8 weeks, blend films start a fragmentation process after only two weeks. Moreover, the influence of the enzymatic degradation in the morphology of the individual polyester and the blend is also very similar to that displayed in Fig. 6 for hydrolytic degradation assays. On the other hand, Fig. 7 shows that the weight loss for the polyester and the blend after 8 weeks of immersion is 3.8% and 22.5%, respectively. These values confirm that the presence of the Lipase F-AP 15 in the degradation medium produces an increment in the weight loss of 2.4% and 5.3% for the polyester and the blend, respectively, with respect to the PBS without enzyme.

Cell adhesion and proliferation

The responses of P3TMA:PE44 nanomembranes towards different cellular lines were compared with those of P3TMA and PE44. Cellular adhesion and proliferation assays were performed considering four different lines of eukaryotic cells: MDCK and Cos-7, which are fibroblast cells, and Du-145 and HEp-2, which are epithelial cells. These carcinogenic cells were selected due to their fast growth. Quantitative results of cellular adhesion assays are displayed in Fig. 8, steel and TCPS being used as control substrates. As can be seen, the number of cells by area of a given material is similar for the four cellular lines. Although the behavior of P3TMA as a supportive matrix for cellular adhesion is significantly worse than that of PE44, the adhesion of fibroblast and epithelial cells on the surface of 50 : 50 nanomembranes is the most favored in all cases.

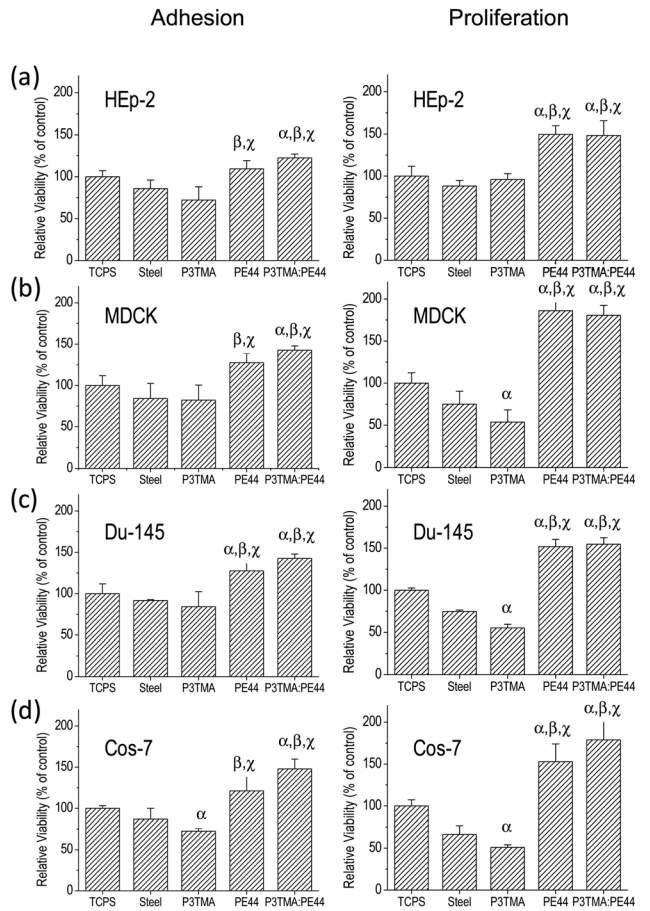

Fig. 8 Cellular adhesion (right column) and proliferation (left column) on P3TMA, PE44 and 50 : 50 P3TMA:PE44 substrates. Assays were carried out using the following eukaryotic cell lines: (a) HEp-2, (b) MDCK, (c) Du-145, and (d) Cos-7. The relative viability was established in relation to the TCPS control (tissue culture polystyrene). Steel was also considered as a control substrate because the individual polymers and the blend were deposited on this material. Greek letters on the columns refer to significant differences ($p < 0.05$) using the ANOVA and Tukey test: α *vs.* TCPS; β *vs.* steel; χ *vs.* P3TMA.

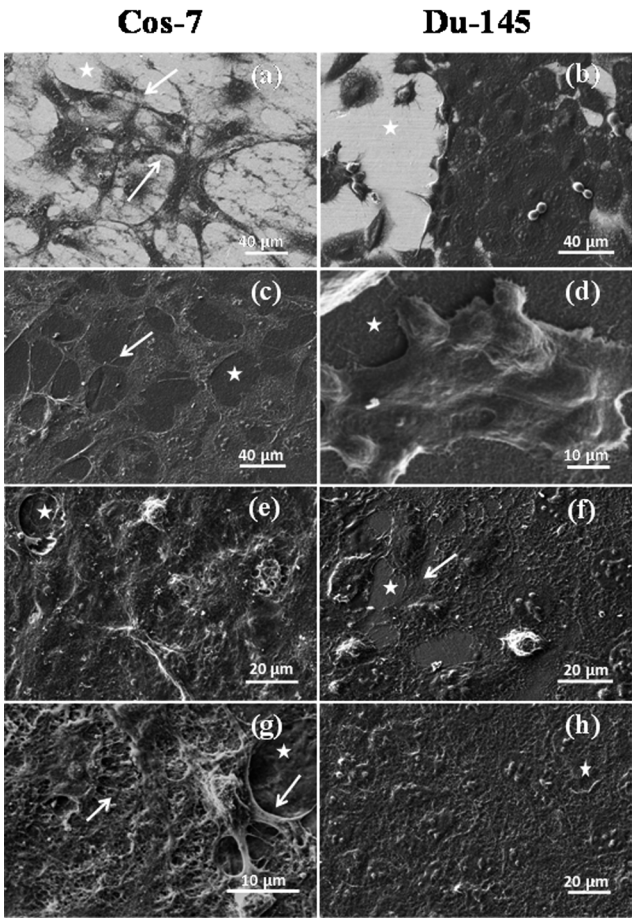

Fig. 9 SEM micrographs of Cos-7 and Du-145 cells adhered on the surface of steel (a and b) and cultured on PE44 (c and d), P3TMA (e and f) and 50 : 50 P3TMA:PE44 (g and h). The substrate surfaces (domains without cells) are shown by asterisks (*), while the connections or interactions between the cell and the surface or between two cells are indicated by arrows.

After 7 days of culture, the cellular activity on the material was re-evaluated. Cellular proliferation results, which are included in Fig. 8, show that the number of viable cells per area of material in the TCPS control substrate remains practically unaltered while that in steel decreases slightly. In contrast, a significant increment in the number of viable cells is detected in both PE44 and 50 : 50 P3TMA:PE44. Indeed, the ability of the two substrates for cellular proliferation is the same for all cellular lines with exception of Cos-7 cells, which show a slight preference towards the blend with respect to the individual polyester. This is an amazing result since the comparison between adhered and proliferated cells reflects in all cases, with exception of HEp-2, the negative behavior of P3TMA as a cellular matrix. Thus, the number of viable cells decreases after seven days of culture for the MCDK, Du-145 and Cos-7 lines. The cell proliferation inhibition exhibited by individual P3TMA should be attributed to the presence of the oxidizing agent ($FeCl_3$) in the matrix, which was in excess during the polymerization process. Thus, recent studies showed both the cytotoxicity effect produced by $FeCl_3$ in MCF-7 cells[50] and the lipid peroxidation induced by this oxidizing agent in the cell membranes.[51] The negative effect induced by $FeCl_3$ is eliminated when the CP is mixed with the polyester because of the reduction in its effective concentration.

Fig. 9 displays SEM images of different cells cultured on steel, P3TMA, PE44 and 50 : 50 P3TMA:PE44 substrates. In general, there is a significant spreading of cells on the surface of steel and PE44 substrates. The connection sites between the cells and the surface of these substrates have been marked with arrows, details about the stress fibers formed by the cells to move along the substrates being also displayed. The latter correspond to the lamellipodia, which are delicate sheet-like extensions of cytoplasm that form transient adhesions with the substrate, and the actin filaments are known as fillopodia (*i.e.* thin extensions of cytoplasm to focal adhesion). The formation of lamellipodia and fillopodia is less abundant on the P3TMA surface, which is consistent with the poor colonization of such a substrate. In contrast, the abundance of cells on the surface of the 50 : 50 blend was so high that it allowed us to identify thick monolayers involving different levels of cellular growth. Similarly, connections of cells to both the blend surface and the neighboring cells

are clearly evidenced in this substrate. Within this context, it should be remarked that Cos-7 cells present a star shape that grow side-by-side forming a very compact monolayer. Such a compact disposition is also observed for Du-145 cells, even though they present a round-like shape. The overall of these *in vitro* results support the fact that 50 : 50 P3TMA:PE444 nanomembranes should be considered as powerful bioactive platforms for tissue regeneration.

Electrobioactivity

The electrochemical behaviour of P3TMA:PE44 nanomembranes coated with MDCK and HEp-2 cell monolayers was investigated by CV in PBS with 0.1 M $LiClO_4$. Fig. 10 compares the control voltammograms recorded for P3TMA, PE44 and 50 : 50 P3TMA:PE44 coated with cellular monolayers with those obtained for the uncovered materials. Although HEp-2 cell monolayers do not affect the profile of the voltammogram recorded for P3TMA and PE44, these epithelial cells produce a slight enhancement of the anodic current densities in both the anodic and cathodic scans. This feature suggests that HEp-2 cells facilitate the ionic diffusivity in the polymer–cells–solution interfaces but do not modify the almost irreversible behaviour of the oxidation processes. In contrast, MDCK cells proliferated on P3TMA and PE44 produce a reduction of the anodic current densities of oxidation and reduction profiles, which causes a loss in the definition of the oxidation peaks that is particularly remarkable for the CP. Accordingly, these cellular line reduces the mobility of the ions at the interfaces, even though as observed for HEp-2 monolayers the irreversible behavior of the oxidation and reduction processes remains unaltered.

The most remarkable effect of the HEp-2 and MCDK cells on the 50 : 50 blend refers to the decrease of the anodic and cathodic intensities in the whole voltammogram, such a reduction being especially evident for the latter monolayers. This feature is particularly striking for the HEp-2 cells since they were found to enhance the anodic and cathodic intensities of the two individual polymers (Fig. 10a and b). The overall of these results suggests that important differences exist in the interfaces of the blend and the individual polymers. Thus, the channels that allow the access and escape of the dopant ions are blocked by the two types of cells in the blends whereas this effect is only detected for MDCK cells in the individual polymers.

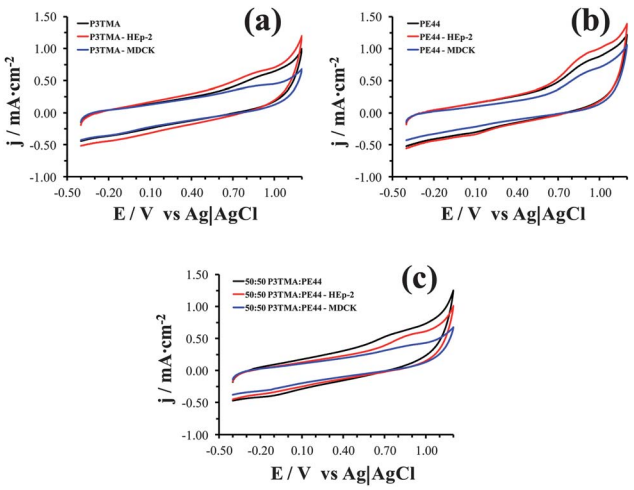

Fig. 10 Control voltammograms of: (a) P3TMA; (b) PE44; and (c) 50 : 50 P3TMA:PE44 in PBS with 0.1 M $LiClO_4$. For each material control voltammograms for the oxidation of the uncoated sample and samples coated with HEp-2 and MDCK cells are displayed.

Fig. 11 displays the SEM micrographs of P3TMA and 50 : 50 P3TMA:PE44 coated with cellular monolayers after eight consecutive oxidation–reduction cycles. As can be seen, cells are severely affected by the electric current, which produces their detachment from the substrate surface. Amazingly, the influence of the electric current in the cellular structure depends on both the substrate and the cellular line. More specifically, the interconnections between the HEp-2 cells and the P3TMA surface (Fig. 11a and b) were damaged by the eight redox processes, whereas damages were not so severe in the case of the 50 : 50 blend (Fig. 11c and d). This result should be attributed to the fact that the initial distribution of cells was very different for the two substrates (*i.e.* see Fig. 11). In opposition, MDCK cells were annihilated by the anodic current in all cases (Fig. 11f and h).

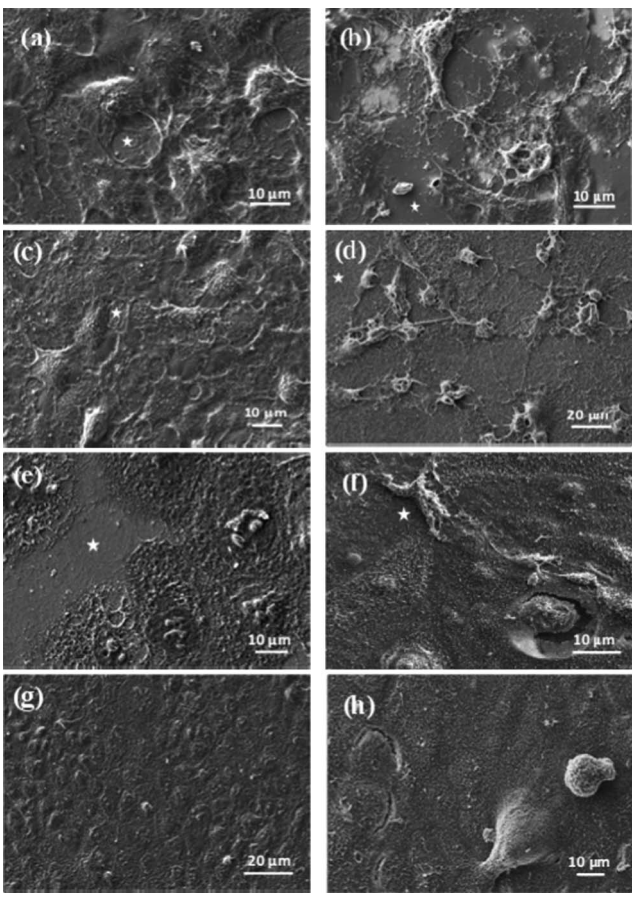

Fig. 11 SEM micrographs of P3TMA and 50 : 50 P3TMA:PE44 samples coated with HEp-2 and MDCK cells before and after an electrochemical treatment consisting of eight consecutive oxidation–reduction cycles: P3TMA coated with HEp-2 cells (a) before and (b) after treatment; 50 : 50 blend coated with HEp-2 cells (c) before and (d) after treatment; P3TMA coated with MDCK cells (e) before and (f) after treatment; and 50 : 50 blend coated with MDCK cells (g) before and (h) after treatment. Stars indicate substrate surfaces not covered by cells.

Thus, although a few isolated cells were detected on the substrates, the surfaces were essentially coated by denatured proteins (*i.e.* cell remainders). It is worth noting that in the initial samples MDCK cells were from compact monolayers (Fig. 11e and g). Therefore, detachment of some cells induced the detachment of neighboring cells, which are in close contact, through a cascade effect. The scenario of HEp-2 cells is completely different since cells are more spread over the surface facilitating their resistance towards the anodic current.

Conclusions

P3TMA:PE44 nanomembranes have been prepared using the procedure developed in our previous work. The flexibility and robustness of the films have been investigated by aspirating the nanomembrane floating in ethanol into a pipette and subsequently releasing it into the solvent. We found that the nanofilm rapidly recovers the original shape, this aspiration/release/shape recovery process being repeated more than five times without producing any damage to the nanofilm. The robustness and flexibility of the nanomembrane have been attributed to the good dispersion of the CP and the polyester in the blend. The structure and wettability of the blend have been investigated and compared with those of the individual polymers using FTIR and contact angle measurements, respectively. Amazingly, both the blend and the individual CP show a very similar hydrophobicity, the contribution of the hydrophilic polyester to the wettability of the 50 : 50 nanomembrane being practically negligible.

Investigation of the electrochemical properties by CV in PBS and acetonitrile indicates that the oxidation and reduction processes found in the individual CP are also present in the blend. Thus, the polyester only affects the infrequent oxidation process detected for P3TMA at 0.22 V, which is blocked in the blend. The electroactivity of both the blend and the P3TMA is higher in acetonitrile than in PBS. Moreover, the definition of the oxidation and reduction peaks is more clear and intense in the organic solvent indicating that in this environment the formation of polarons is more localized. However, the electrochemical stabilities of the blend are similar in the physiological and the organic environments.

Hydrolytic and enzymatic degradation produce changes in the superficial texture of the PE44 samples, which are evidenced by the appearance of crevasses and thin grooves. In spite of this, the weight loss was very low in both cases since the degradation media only penetrate into the amorphous domains of the polyester. In contrast, the weight loss grows significantly when the 50 : 50 blend is exposed to hydrolytic and, especially, enzymatic degradation media, which has been attributed to the fact that the degraded polyester facilitates the detachment of the P3TMA domains. Thus, the degradation rate is considerably higher for the blend than for the individual polyester. Cellular adhesion and proliferation assays have been carried out using the HEp-2, MDCK, Cos-7 and Du-145 lines. Results clearly evidence that the 50 : 50 blend behaves as a potent cellular matrix, the viability of the cultured cells being significantly higher in the blend than in polyester and, especially, the CP. Indeed, cellular proliferation is inhibited by the PT3MA substrate, which has been attributed to the detrimental effects caused by an excess of $FeCl_3$. Moreover, proliferation assays using MDCK, Cos-7 and Du-145 cells indicate that the potential applicability of the blend as a bioactive platform for tissue regeneration is higher than that proposed in our preliminary study using HEp-2 cells,[35] which clearly showed the worst behaviour.

Analysis of the electrobioactivity of P3TMA, PE44 and the 50 : 50 blend coated with HEp-2 and MDCK monolayers has been carried out using CV. Comparison of the results obtained for uncoated and coated systems indicates that all three materials are electrocompatible with cellular monolayers, even though the anodic and cathodic intensities are in general smaller for the coated systems. On the other hand, inspection of the cellular connections after eight consecutive oxidation and reduction cycles indicates that the HEp-2 cells are more resistant towards the anodic current than the MDCK ones. The different electrobioactive behavior found for HEp-2 and MDCK lines suggests a significant dependence on the interaction between cells and the substrate surface. In summary, the combination of P3TMA and PE44 to produce nanomembranes allows us to retain, or even to improve, the best properties of each individual material (*i.e.* biodegradability and behavior as cellular matrix of PE44 and electroactivity of P3TMA).

Acknowledgements

Financial support from the MICINN and FEDER (MAT2009-09138) and Generalitat de Catalunya (research group 2009 SGR 925 and XRQTC) is gratefully acknowledged. Support for the research of C.A. was received through the prize "ICREA Academia" for excellence in research funded by the Generalitat de Catalunya. M. M. P. M. thanks the financial support through a FPI-UPC grant.

References

1 M. Mazzeo, V. Vitale, F. Della Salla, M. Anni, G. Barbarella, L. Favaretto, G. Sotgiu, R. Cingolani and G. Gigli, *Adv. Mater.*, 2005, **17**, 34.
2 W. U. Huynh, J. J. Dittmer and A. P. Alivisatos, *Science*, 2002, **295**, 2425.
3 P. Bjork, D. Thomsson, O. Mirzov, J. Wigenius, O. Inganas and I. Scheblykin, *Small*, 2009, **5**, 96.
4 H. A. Ho and M. Leclerc, *J. Am. Chem. Soc.*, 2004, **126**, 1384.
5 M. Hamedi, R. Forchheimer and O. Inganas, *Nat. Mater.*, 2007, **6**, 357.
6 R. Berridge, S. P. Wright, P. J. Skabara, A. Dyer, T. Steckler, A. A. Argun, J. R. Reynolds, W. H. Ross and W. J. Clegg, *J. Mater. Chem.*, 2007, **17**, 225.
7 R. A. Marsh, J. M. Hodgkiss and R. H. Firend, *Adv. Mater.*, 2010, **22**, 3672.
8 N. K. Guimard, N. Gomez and C. E. Schmidt, *Prog. Polym. Sci.*, 2007, **32**, 876.
9 A. Mishra, C. Q. Ma and P. Bäuerle, *Chem. Rev.*, 2009, **109**, 1141.
10 H. S. O. Chan and S. C. Ng, *Prog. Polym. Sci.*, 1998, **23**, 1167.
11 G. Barbarella, M. Melucci and G. Sotgiu, *Adv. Mater.*, 2005, **17**, 1581.
12 T. A. Chen, X. Wu and R. D. Rieke, *J. Am. Chem. Soc.*, 1995, **117**, 233.
13 C. Yang, F. P. Orfino and S. Holdcroft, *Macromolecules*, 1996, **29**, 6510.
14 R. D. McCullough, *Adv. Mater.*, 1998, **10**, 93.
15 M. Chayer, K. Faïd and M. Leclerc, *Chem. Mater.*, 1997, **9**, 2902.
16 B. Kim, L. Chen, J. Gong and Y. Osada, *Macromolecules*, 1999, **32**, 3964.
17 D. J. Liaw, B. Y. Liaw, J. P. Gong and Y. Osada, *Synth. Met.*, 1999, **99**, 53.
18 P. C. Ewbank, R. S. Loewe, L. Zhai, J. Reddinger, G. Sauvé and R. D. McCullough, *Tetrahedron*, 2004, **60**, 11269.

19 O. Bertran, E. Armelin, J. Torras, F. Estrany, M. Codina and C. Alemán, *Polymer*, 2008, **49**, 1972.
20 E. Armelin, O. Bertran, F. Estrany, R. Salvatella and C. Alemán, *Eur. Polym. J.*, 2009, **45**, 2211.
21 O. Bertran, E. Armelin, F. Estrany, A. Gomes, J. Torras and C. Alemán, *J. Phys. Chem. B*, 2010, **114**, 6281.
22 K. H. Hsieh, K. S. Ho, Y. Z. Wang, S. D. Ko and S. C. Fu, *Synth. Met.*, 2001, **123**, 217.
23 M. E. Nicho, D. Peña-Salgado and P. Altuzar-Coello, *Thin Solid Films*, 2010, **518**, 1799.
24 A. Özgün, B. Sari, A. Uygun, H. I. Ünal and Ç. Çakanyildirim, *Int. J.Polym. Anal. Charact.*, 2009, **14**, 469.
25 S. Manna, A. Mandal and A. K. Nandi, *J. Phys. Chem. B*, 2010, **114**, 2342.
26 D. Mawad, K. Gilmore, P. Molino, K. Wagner, P. Wagner, D. L. Officer and G. G. Wallace, *J. Mater. Chem.*, 2011, **21**, 5555.
27 G. G. Wallace and L. A. P. Kane-Maguire, *Adv. Mater.*, 2002, **14**, 953.
28 J. Hu, L. Huang, X. Zhuang, P. Zhang, L. Lang, X. Chen, Y. Wei and X. Jing, *Biomacromolecules*, 2008, **9**, 2637.
29 Q.-S. Zhang, Y.-H. Yan, S.-P. Li and T. Feng, *Biomed. Mater.*, 2009, **4**, 035008.
30 L. J. del Valle, D. Aradilla, R. Oliver, F. Sepulcre, A. Gamez, E. Armelin, C. Alemán and F. Estrany, *Eur. Polym. J.*, 2007, **43**, 2342.
31 L. J. del Valle, F. Estrany, E. Armelin, R. Oliver and C. Alemán, *Macromol. Biosci.*, 2008, **8**, 1144.
32 D.-F. Li, H.-J. Wang, J.-X. Fu, W. Wang, X.-S. Jia and J.-Y. Wang, *J. Phys. Chem. B*, 2008, **112**, 16290.
33 R. D. Breukers, K. J. Gilmore, M. Kita, K. K. Wagner, M. J. Higgins, S. E. Moulton, G. M. Clark, D. L. Officer, R. M. I. Kapsa and G. G. Wallace, *J. Biomed. Mater. Res., Part A*, 2010, **95**, 256.
34 T. J. Rivers, T. W. Hudson and C. E. Schmidt, *Adv. Funct. Mater.*, 2002, **12**, 33.
35 E. Armelin, A. L. Gomes, M. M. Pérez-Madrigal, J. Puiggalí, L. Franco, L. J. del Valle, A. Rodríguez-Galán, J. S. de C. Campos, N. Ferrer-Anglada and C. Alemán, *J. Mater. Chem.*, 2012, **22**, 585.
36 T. Fujimaki, *Polym. Degrad. Stab.*, 1998, **30**, 209.
37 R. Vendamme, S. Y. Onoue, A. Nakao and T. Kunitake, *Nat. Mater.*, 2006, **5**, 494.
38 H. Watanabe, T. Ohzono and T. Kunitake, *Macromolecules*, 2007, **40**, 1369.
39 H. Watanabe and T. Kunitake, *Adv. Mater.*, 2007, **19**, 909.
40 T. Mosmann, *J. Immunol. Methods*, 1983, **65**, 55.
41 B. Teixeira-Dias, L. J. del Valle, F. Estrany, J. F. Mano, R. L. Reis and C. Alemán, *Macromol. Mater. Eng.*, 2011, **296**, DOI: 10.1002/mame.201100180, in press.
42 P. N. Bartlett and D. H. Dawson, *J. Mater. Chem.*, 1994, **4**, 1805.
43 E. W. Fischer, H. J. Sterzel, G. Wegner and Z. Z. Kolloid, *Polymer*, 1973, **251**, 980.
44 F. Von Burkersroda, L. Schedl and A. Göpferich, *Biomaterials*, 2002, **23**, 4221.
45 J. A. Tamada and R. Langer, *Proc. Natl. Acad. Sci. U. S. A.*, 1993, **90**, 552.
46 R. A. Kenley, M. O. Lee, T. R. Mahoney and L. M. Sanders, *Macromolecules*, 1987, **20**, 2398.
47 M. Hakkarainen, A. C. Albertsson and S. Karlsson, *Polym. Degrad. Stab.*, 1996, **52**, 283.
48 H. Antheunis, J.-C. Van der Meer, M. De Geus, A. Heise and C. E. Koning, *Biomacromolecules*, 2010, **11**, 1118.
49 H. Antheunis, J.-C. Van der Meer, M. De Geus, W. Kingma and C. E. Koning, *Macromolecules*, 2009, **42**, 2462.
50 E. Laqué-Rupérez, M. J. Ruiz-Gómez, L. de la Peña, L. Gil and M. Martínez-Morillo, *Bioelectrochemistry*, 2003, **60**, 81.
51 K. J. Woollard, S. Sturgeon, J. P. F. Chin-Dusting, H. H. Salem and S. P. Jackson, *J. Biol. Chem.*, 2009, **284**, 13110.